Development of Cardiac Troponin I Electrochemical Impedance Immunosensor

Meng Xiong[*], *Xihua Wang, Yanan Kong and Bin Han*

Zhongda Hospital, Southeast University, Nanjing, Jiangsu, 210000, P. R. China
[*]E-mail: mengxiong_nanjing@yahoo.com

It is well known that acute myocardial infarction (AMI), a type of heart attack, is a primary cause of sudden death that has high potential to lead to nonreversing damage or necrosis of myocardial tissues. In this easy, we focused on the biosynthesis of Ag nanoparticles with the employment of green algae Stoechospermum marginatum as a reductant. The whole course of synthesis was fast in which the development of Ag nanoparticles was accomplished less than 1 hour after the chemical reaction between Ag salt and algal extract. After this, the AgNPs were utilized for the formation of electrochemical impedance cardiac troponin I immuno-transducer.

1. INTRODUCTION

Cardiovascular diseases (CVDs) generally refer to a range of diseases, like congenital heart defect, rheumatic pancarditis, pulmonary embolism characterized as the imbalance of heart and blood vessels. It is reported by the World Health Organization (WHO) that approximately 31% (17.5 million) of deaths all over the world in 2012 were resulted from CVDs, which means that CVDs is the primary cause of global deaths[1, 2]. The appearance of CVDs can be attributed to several factors, such as age, pressure, heredity, high blood pressure, etc. [3, 4]. Early discovery and treatment of CVDs is very critical for life-saving as well as time-saving of patients [5]. Human cardiac troponin I (cTnI) is regarded as the gold standard marker of cardiac trauma due to its high sensitivity in the diagnosis of acute myocardial infarction (AMI). In the previous phase of myocardial disease, the detection of cTnI at super low concentration plays a critical role in the precognition and classification of the cardiac diseases. When AMI is initiated, the concentration of cTnI in blood rises with high speed within 3 to 4 hours. In order to determine cTnI in the lab, it is advisable to adopt enzymatic immunoassay on the

basis of chemiluminescent substrates' reaction with cTnI [6-9]. Compared to other cTnI determination approaches, point-of-care test has a cutting edge that is it can be adopted as a favorable diagnostic tool to save testing time. As a result, immunosensor with immunoassay can be applied for the determination of cTnI in emergency room conveniently and effectively.

Based on the reaction of antigen and antibody, immunoassay, an analytical approach, has been employed by researchers to detect protein biomarkers quantitatively [10-12]. Recently, a variety of immunoassays classified based on various approaches of transducing signals play a great role in the determination of protein markers. There are several immunoassay tools, among which the most widely used are spectroscopy, colorimetric, electrochemistry and chromatography analysis [13-17]. Among the aforementioned methods, electrochemistry has an great advantage over others owing to its high sensitivity and cheapness, which can be adopted free from complicated equipment [18, 19]. There are two aspects which should be emphasized to make this approach more advanced. On the one hand, an effective label to form signals can be made to amplify signals, making the detection and quantification much easier[20].There is no doubt that new instruments and approaches related to the analysis will appear in the future, owing to prospective nanomaterial technological size, as well as their improvement in various aspects[21-23].

In recent years, there are a large number of researchers who have committed themselves in the study of electrochemical impedance spectroscopy (EIS). It has excellent sensitivity free from any damage in the electrical perspective. Moreover, it can speed up the biology processes, such as the development of biotin–avidin or antigen–antibody and the reaction between DNA and oligonucleotides [24-26]. With the purpose of detecting cTnI, this essay issues a base to product bioelectrode through the combination of the advantages of both Ag NPs developed in biosynthesis and EIS. In the covalent form, the Ag NPs processed in the biosynthesization process are fastened to a 3-aminopropyltriethoxy silane (APTES) self-assembled monolayer (SAM) with an indium-tin-oxide (ITO)-glass plate platform. As the antibody with respect to cardiac protein, Ab-cTnI sticked on APTES/ITO-glass plates processed by the modification of AgNPs as well as the functionalization of carboxyl in the covalent form. The realization of it was attributed to a carbodiimide coupling reaction. This type of bioelectrodes was characterized by various approaches relevant to the microscope. At the same time, with the use of the probe for redox, the bioelectrode, undertaken by $[Fe\,(CN)_6]^{3-/4-}$, has been studied concerning its immunosensing capacity employed to estimate Ag-cTnI in phosphate buffer saline (PBS; pH 7.4) quantitatively.

2. EXPERIMENTAL

2.1. Chemicals and instruments

The supplier of native cTnI extracted from myocardium tissue of human was Chenxinbio. The materials used in this process came from Sigma-Aldrich Corp, including *N*-hydroxy succinimide 98% (NHS), $AgNO_3$, sodium borohydride ($NaBH_4$), mouse monoclonal anti-cTnI, 3-Aminopropyl triethoxysilane (APTES), *N*-(3-Dimethyl aminopropyl)-*N'*-ethyl carbodiimide hydro chloride

(EDC)and 3-mercaptopropionic acid (MPA). The morphology of the surface of the electrode was analyzed by scanning electron microscopy (JSM-6700F field emission scanning electron microscope, JEOL Ltd., Japan). Fourier transform infrared (FTIR) spectroscopy was performed using a Perkin Elmer FTIR spectrometer (RX). Spectrophotometrically (JASCO V/560 UV/Vis, Japan) with the wavelength of 525 nm was employed for the laccase activity measurement. The XRD with Cu Kα radiation (D8-Advanced, Bruker, Germany) was employed to characterize the crystal phase information of the sample from 5 to 80 in 2θ. The X-ray photoelectron spectroscopy (XPS) was performed on a Kratos AXIS Nova (UK) spectrometer.

2.2. Biosynthesis of Ag NPs

The synthesis of Ag NPs that were put into 0.1L water, 10g powder of *Stoechospermum marginatum* passed sonication for three quarters and heat treatment under70 ^{o}C for another three quarters. Later, filter paper with 200nm pore size was applied to filtrate the exact of *Stoechospermum marginatum.* The combination of AgNO$_3$ solution (20 mL) with *Stoechospermum marginatum* extract (20 mL) led to the formation of Ag nanoparticles in the synthesis process. And then, the synthesized nanoparticles underwent 1 hour's sonication. The generation of Ag nanoparticles was revealed through the change of the solution color from light yellow to purplish yellow. Before the start of the washing section, 10,000 rpm centrifugation was used for the dissociation for half hour. The obtained Ag nanoparticles underwent drying inside an over at 70°C. The way Ag NPs was functionalized was manifested in the next processes. Then, H$_2$O (10 mL) blended with MPA (46 μL) was added in rapidly to main the stabilization of the Ag NPs solution, with 50 ml in the final. This mixture was being stirred for 2 hours at operating temperature to be become colloid, and then, it underwent 2-3 times washing with the use of ethanol, centrifugation at 20000 rpm, and also drying under vacuum for half a day.

2.3. Preparation of electrochemical immunosensor

Before the initiation of drying under vacuum, the glass plates covered with ITO underwent sanitary disposal through ultrasonic in order. Aiming to get a large number of hydroxyl species on the surface of ITO-glass, the plates were exposed to oxygen plasma for five minutes. And then, for the purpose of obtaining APTES's SAM, the plates were immersed into APTES solution with ethanol whose concentration was 2% under indoor environment. Then ethanol was used to water these products, so as to let the substrate free from un-bonded APTES. When this was finished, stream of nitrogen was used for drying. As for the ITO glass plates which have undergone APTES's modification for 3 hours, the receiver was undertaken by the prepared solution mixture of Ag(MPA) nanoparticles functionalized. The Ag(MPA-NHS)/APTES/ITO-glass was obtained by further drying with the stream of nitrogen and rinsing through water that has been distilled for two times. Before this, Ab-cTnI was treated with PBS with Ab-cTnI of 100 μg/mL for one night under the temperature of 4 °C, and then being fastened on the prepared electrode. Later, as for impeding non-particular bonding points on the electrode surface, the prepared electrode was incubated in the solution of BSA whose

concentration was 1% for 2 quarters, followed by rinsing with the adoption of PBS for the purpose of getting over all potential antibodies physically adhering to it. Then through the stream of nitrogen, the dried form of it was formed.

2.4. Electrochemical immunoassay

The determination of cTnI was achieved in the electrochemistry perspective using a triple-electrode set in which a Pt foil was adopted to develop a counter electrode, whereas a reference electrode through a saturated Ag/AgCl. 2 mM $[Fe(CN)_6]^{3-}$/$[Fe(CN)_6]^{4-}$ within the frequency scope of 1 Hz-100 kHz at an AC voltage of 0.05V made the implementation of the electrochemical impedance spectroscopy successful. In PBS, same portions with different concentrations obtained from the previous 100 μg/mL Ag- cTnI solution were formed. In the Ab-cTnI/Ag(MPA)/APTES/ITO-glass bioelectrode, these portions were added in, and then the response was measured. A solution free from Ag-cTnI made a measurement approach with respect to impedance possible. At the time that a Nyquist pot severed as an initiation for investigating electron transfer resistance (R_{et}), the response of the control specimen was accomplished. After this, with the immunoreaction between the antibody and antigen, an advanced detection was used which measured relevant EIS parameters, such as R_{et} equal portions with different concentrations.

3. RESULT AND DISCUSSION

The reaction relevant to biosynthesis started when Stoechospermum marginatum extracted from $AgNO_3$ solution was added. It could be observed that the color of the dispersed solution changed from light yellow to purplish yellow, revealing the nucleation of Ag nanoparticles. Owing to the fact that the dispersion and absorption of light would take place because of the particles' metallic properties, AgNPs' plasmon resonances on the cover inside the solution could be observed. The optical performance could be affected by three factors, namely the form, size and solvent. *Stoechospermum marginatum* made the synthesis of AgNPs possible. The UV-vis spectrum of AgNPs could be seen in Figure 1 in which the observation of an outstanding absorption crest as well as AgNPs's appearance plasmon resonance could be realized. This state offered sufficient evidence for the fact that metallic gold was produced. The average size of prepared AgNPs was in accordance with the location of appearance plasmon resonance crest. Early research showed that the size of AgNPs which underwent biosynthesis was predicted to be 20-80 nm. With the adoption of scanning electron microscopy (SEM), the as-prepared AgNPs passed through biosynthesis showed a globe form with little accumulation, which could be seen in Figure 1B. After the observation of this figure, it could be seen that there was coherence in the size of AgNPs which underwent the synthesis with the addition of *Stoechospermum marginatum*. The size distribution of the Ag nanoparticles was also characterized using DLS. The DLS pattern displays the mean size distribution of Ag nanoparticles was 47.7 nm. Moreover, the

polydispersity index of the Ag nanoparticles had been found to be 0.922, which could form a well dispersed colloidal solution [27].

The formation of AgNPs was proved by X-ray photoelectron spectroscopy. It can be seen from Figure 2A that the observation of AgNPs after biosynthesis could be achieved easily through XPS, with the $Ag_{3d3/2}$ and $Ag_{3d\ 5/2}$ crests filed at 374.7 and 368.4 eV accordingly [28, 29]. Owing to the adherence of biomolecules, a variation of Ag^0's figure occurred theoretically on 87.7 eV and 84.0 resulted from the extraction of *Stoechospermum marginatum* as shown in the crests.
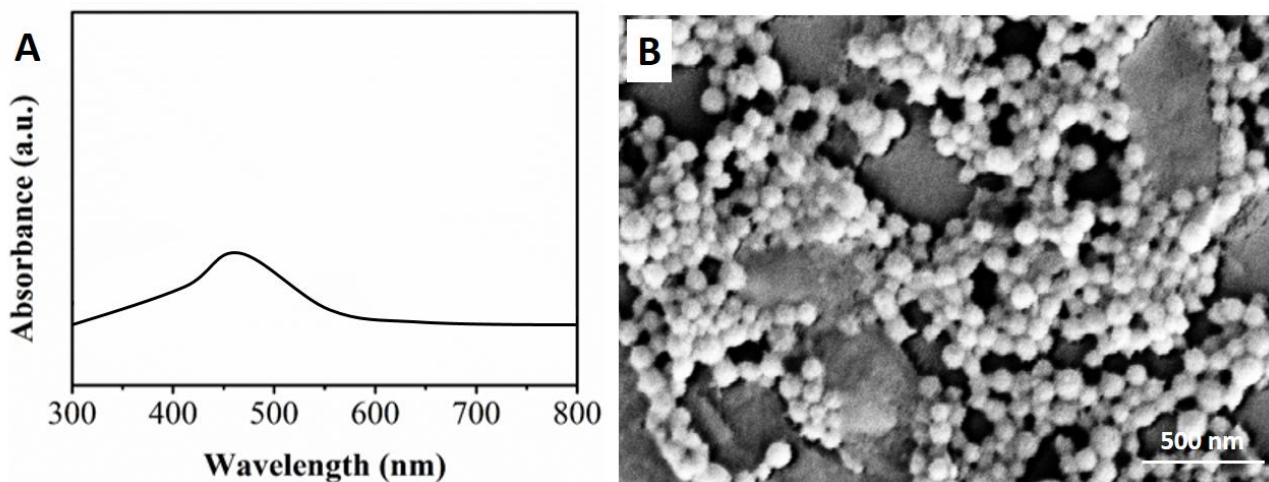
Figure 1. (A) UV-vis spectrum as well as (B) SEM image of AgNPs after biosynthesis.
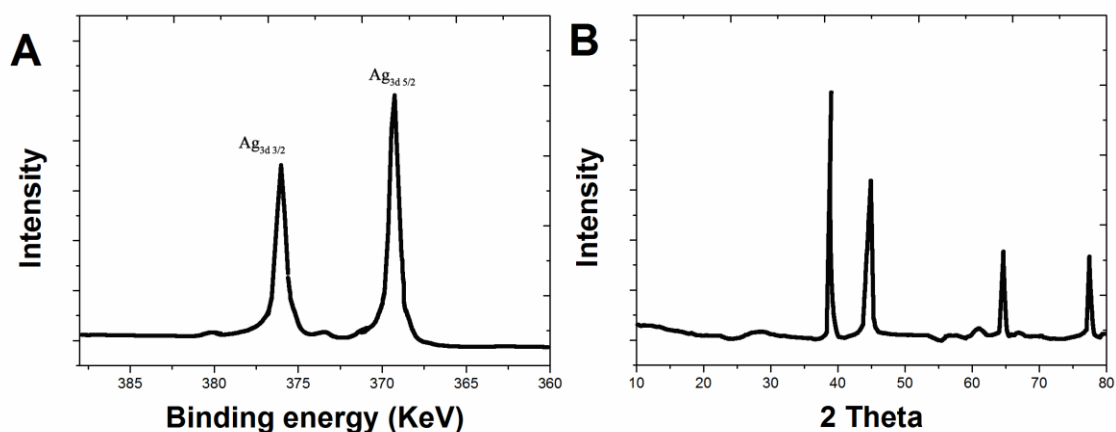

Figure 2. (A) High resolution Ag 4f scan as well as (B) XRD pattern of Ag nanoparticles after biosynthesis.

Figure 2B demonstrated X-ray diffraction spectra of AgNPs which underwent biosynthesis, showing that there were four crests of AgNPs, and the location was 39.2°, 45.8°, 67.6° and 81.8° accordingly. These crests were in accordance with (111), (200), (220) as well as (311) planes of face-centered-cubic (fcc) crystallographic framework of Ag (JCPDS 4-0783) accordingly. The (111) plane

shows the highest intensity among all crystal planes, suggesting that silver is preferable to grow in (111) planes under the galvanic replacement condition. The (111) plane is also known as the most stable crystal plane of Ag [30].

Fourier Transform Infrared pattern of the Ag-cTnI/Ag(MPA)/APTES/ITO as well as APTES/ITO Ag(MPA)/APTES/ITO with attenuated total reflection (ATR) could be seen in Figure 3. This pattern reveals the typical Si–O–Si bond in accordance with APTES at 1051 cm^{-1}. The crest was detected at 1744 cm^{-1} in that AgNPs after MPS-functionalization made their carboxylic species vibrate stretching for C=O. Two crests whose locations were 2962 cm^{-1} and 937 cm^{-1} respectively were in accordance with the carboxylic acid species' –OH vibrations that were both stretching and bending. Extra crests at 1613 cm^{-1} and 3385 cm^{-1} revealed N–H bending and stretching vibrations. Before this, the fixation of Ab-cTnI had appeared. The aforementioned situation showed that Ab-cTnI molecules produced amide bond as well as Ag(MPA) nanoparticles.
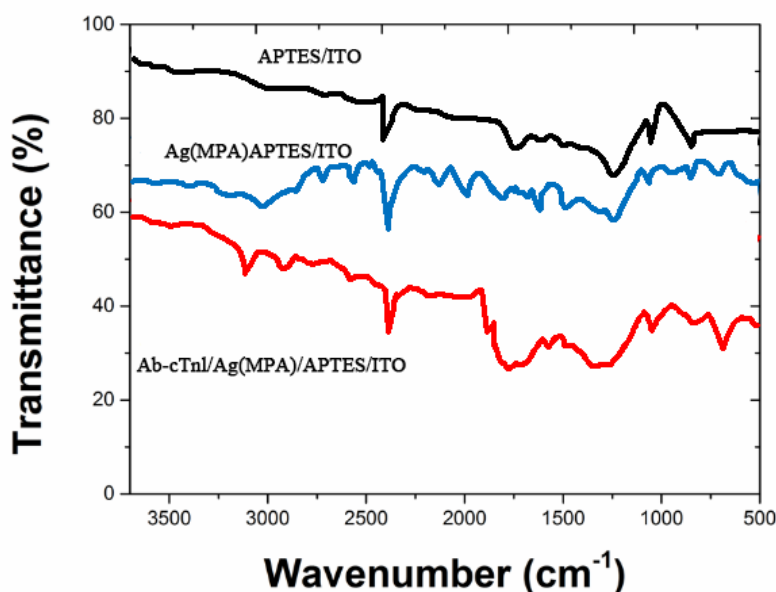
Figure 3. FTIR spectra of APTES/ITO-glass Ag(MPA)/APTES/ITO-glass as well as Ab-cTnI/Ag(MPA)/APTES/ITO-glass.

EIS, as a versatile approach for the characterization of reactions with respect to electrochemisty which occurred on the electrode having undergone modification, has a cutting edge over other counterparts in this area. EIS detects the way the researched mechanism responded when a small amplitude AC signal of different frequencies was employed. This kind of method is unable to identify the chemical intermediates or bonds, it can offer critical clues relevant to the probability of reaction occurring between the electrode and the solution, which is usually realized with the use of an 'equivalent circuit'. The functionalization of a series of electrical components in this circuit was achieved with the solution as well as electrode mode characterized by its physioelectric advantages. In detail, in this experiment, Randles equivalent circuit model was employed, which was constituted by the factors as follow: (1) the electron-shift resistance, R_{et}; (2) the Warburg impedance, Z_w, resulted from the dispersion of ion from the bulk electrolyte to the interface of the electrode; (3) the interfacial

dual layer capacitance (C_{dl}) at the interface of electrode/solution with respect to the electrode's appearance state and the plain resistance of the electrolyte solution R_s. Constant phase element, also known as CPE, has been adopted for the improvement of this mode through replacing its previous capacitance, making the Helmholtz dual layer's union and enabling the roughness of electrode appearance with heterogeneity. The CPE is added parallel to both R_{et} and $Z_{w.}$. There is a set of arrangements with R_s for these three elements mentioned before. The impedance relevant to CPE is stated as follows: $Z_{CPE}(\omega) = 1/Y_0(j\omega)^n$.

In this formula, Y_0 and j represent a constant and an imaginary number respectively, while ω and n are on behalf of the angular frequency and the CPE exponent that can not only be adopted as one gauge of the heterogeneity, but also be used to offer details related to the surface inhomogeneity degree. According to the value of n, CPE has the ability to represent the resistance, capacitance ($Y_0 = C$, $n = 1$), inductance ($n = -1$) or Warburg element ($n = 0.5$). The exponent's values approached 1, which showed minimal flaws in the layer of medication on the appearance of the electrode. In this work, it also showed that CPE looks like a phony capacitor. The impedance action of diverse modified electrodes was manifested through Nyquist plots (the genuine section of the impedance Z' *vs.* the imaginary section$-Z''$).

These plots mainly show dual critical regions: one is a semicircle whose frequencies are high, revealing the course of Faradaic electron transfer where the semicircle diameter is equivalent to R_{et}; the other is a straight region whose frequencies are lower, describing the redox species' confusion confinement from the electrolyte to the interface of the electrode. Low values of χ2 of the 10^{-4} order were gained, showing that the fitting circuit pattern chosen could offer promising results. Nyquist plots for diverse modified electrodes which have the same circuits revealed as insets can be manifested in Figure 4. The vacant ITO-glass indicates the R_{et} value is 82.55 Ω cm^2, and this value is quickly declined to 23.19 Ω cm^2 for the APTES/ITO-glass. In other words, the successful immobilization of cTnIs was confirmed with increased *Rct*. Similarily, the observed increase of *Rct* also confirmed the successful decoration of the blocking agent on the electrode surface [31]. This signifies a facile electronic transfer at the interface of the electrode surface. The decline of the R_{et} value with a relatively great Y_0 value of 4.82 µF/cm is caused by the uplifted concentration of the anionic probe $[Fe(CN)_6]^{3-/4-}$ at the interface on account of its great affinity to the polycationic layer as APTES's amino groups which are protonated (NH_3^+) in aqueous aqua. When the Ag(MPA)-NPs covalently adhered to the silane layer, R_{et} elevated to 99.5.0 Ωcm^2 quickly, and because of the charge repulsive behavior of Ag(MPA)-NP carboxyl groups being conversely charged at pH 7.4 to the anionic probe at the interface of electrode/solution, Y_0 was declined to 3.04 µF/cm^{-2} .

In order to determine that there were carboxyl groups at the appearance of the electrode modified, this paper implemented EIS research on an Ag NPs (without MPA capping) modified APTES/ITO-glass electrode free from the functionalization of carboxyl. It can be found in the corresponding Nyquist plot that the semicircle's diameter together with R_{et} declined, and the latter declined to 9.0 Ω cm^2 , revealing that free transport of electrons from the probe to the appearance of the electrode. In the Ag(MPA)-NP-modified electrode, there showed a very high relative signal variation in comparison with that in the AgNPs-modified electrode, providing sufficient evidence for

the large number of unconstrained free carboxyl groups on the appearance of the Ag/(MPA)/APTES/ITO-glass electrode. Moreover, the R_{et} value was improved to 179.6 Ω cm^2, while the Y_0 was declined to 2.39 μF/cm^2 resulted from covalent immobilization of heart cTnI protein antibody over the appearance of the electrode as well as the following obstruction of the common binding sites through BSA. Through this, the insulating behavior of the protein molecule that constrained not only the charge but also the mass transport of the probe towards the surface of the electrode was manifested.
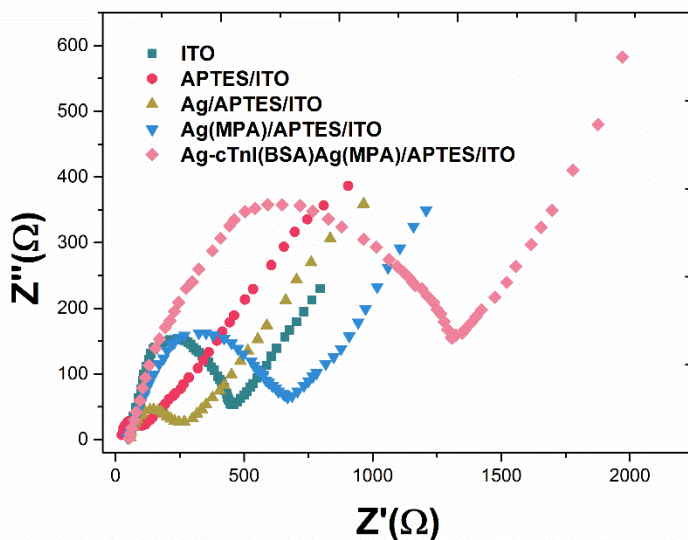
Figure 4. (A) Nyquist plots gained for vacant ITO glass plate; Ag(MPA)/APTES/ITO-glass; APTES/ITO-glass; Ag/APTES/ITO-glass as well as Ag-cTnI(BSA)/Ag(MPA)/APTES/ITO-glass in PBS (pH 7.4, 0.1 M KCl) comprising 2 mM [Fe(CN)$_6$]$^{3-}$/$^{4-}$
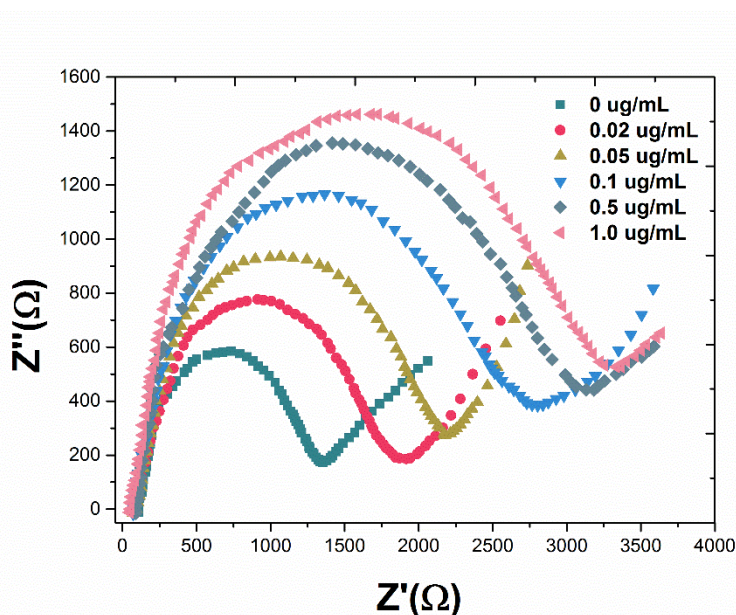
Figure 5. Faradaic impedance spectra of the Ab-cTnI(BSA)/Ag(MPA)/APTES/ITO-glass electrode before and after incubation with diverse concentrations of Ag-cTnI in PBS (pH 7.4) with 0.1 M KCl solution comprising 2 mM [Fe(CN)$_6$]$^{3-/4-}$.

Owing to the particular immunoreaction of Ab-cTnI towards the complimentary objective Ag-cTnI at the appearance of the electrode, an compound of antibody and antigen was developed, leading to the formation of one kinetic impediment that disturbed the transfer of interfacial electrode on the cover of the bioelectrode/solution. With the growing obstruction on the Faradaic reaction of one redox couple, the capacitance declines, while the electron transfer resistance elevates correspondingly. Ag-cTnI, the specimen solution free from a target protein was employed to be the control specimen, while the response of the control specimen was undertaken by the R_{et} value accordingly.

Figure 5 is the demonstration of Nyquist plots acquired when continuous aliquots of diverse concentrations of the objective protein antigen were put in. Through the observation, it can be seen that there is a noticeable elevation in the Nyquist circles' diameter with growing Ag-cTnI dosage resulted from the interaction between antigen and antibody. A slight while still noticeable decline in Y_0 was seen as well, signifying a decline in the capacitive reaction of the bioelectrode with immunoreaction. The sensitivity of the proposed sensor was compared with that of other reported cTnI sensors and the results were presented in Table 1.

Table 1. Comparison of the present immunosensor with other cTnI sensors.

Electrode	Linear detection range	Detection limit	Reference
AuNPs co-immobilized on a dithiol-modified surface	0.003 to 0.5 ng/mL	0.0015 ng/mL	[32]
Carbon nanotube-based electrochemical immunosensor	0.1 to 10 ng/mL	0.033 ng/mL	[33]
SPR immunosensor	0.03 to 6.5 ng/mL	0.01 ng/mL	[34]
Silicon nanowire clusters-metal-oxide	—	1 fg/mL	[35]
Sandwich immunoassay with AuNPs as fluorescence quenchers	60 to 660 ng/mL	0.7 ng/mL	[36]
Glycine/anti-cTnT/graphene/SPE	0.02 to 1 ug/mL	0.001 ug/mL	This work

By describing the variation in specialized electron charge transfer resistance ($\Delta R_{et} = (R_{et})_{after\ immunoreaction} - (R_{et})_{control}$) *vs.* the logarithmic value of Ag-cTnI concentration within the scope of 20 ng/mL-1 µg/mL, the sensitivity of the bioelectrode was acquired. The detection limit was figured out to be 5.5 ng/mL, which was treble the ratio of signal-to-noise. In the process of the EIS experiment, the entire assay needs approximately 12 min, containing 3 min for the preparation of specimens free from any early treatment (in comparison with a couple of days for ELISA), revealing its perspective usage for the previous AMI detection. All of these manifests that compared to semiconductor/metal nanoparticle/carbon nanomaterials as well as cTnI sensors on the basis of polymer, the bioelectrode is more advantageous owing to its physiological scope for cTn1 determination with minimal preparation time of specimens and experimental procedures as well as excellent sensitivity.
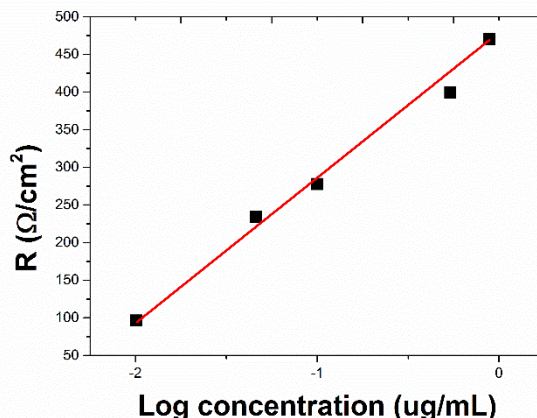
Figure 6. Concentration dependent calibration profile of the bioelectrode.

4. CONCLUSION

In this research, we put forward a biosynthesis approach towards AgNPs preparation with the use of *Stoechospermum marginatum* as a reductant. And then, the AgNPs after biosynthesis was adopted for EIS characterization of a bioelectrode towards the cTn1 clinical levels' detection for the diagnostics of AMI. On account of the broad linear scope and low LOD, the immunosensor being raised revealed better performance that electrochemical immunosensors reported early.

References

1. D. Ettehad, C. Emdin, A. Kiran, S. Anderson, T. Callender, J. Emberson, J. Chalmers, A. Rodgers and K. Rahimi, *The Lancet*, 387 (2016) 957.
2. L. Müller, C. Caris-Veyrat, G. Lowe and V. Böhm, *Critical Reviews in Food Science and Nutrition*, 56 (2016) 1868.
3. M. Al-Mallah, I. Farah, W. Al-Madani, B. Bdeir, S. Al Habib, M. Bigelow, M. Murad and M. Ferwana, *Journal of Cardiovascular Nursing*, 31 (2016) 89.
4. A. Wahid, N. Manek, M. Nichols, P. Kelly, C. Foster, P. Webster, A. Kaur, C.F. Smith, E. Wilkins and M. Rayner, *Journal of the American Heart Association*, 5 (2016) e002495.
5. D. Aune, N. Keum, E. Giovannucci, L. Fadnes, P. Boffetta, D. Greenwood, S. Tonstad, L. Vatten, E. Riboli and T. Norat, *BMC Medicine*, 14 (2016) 207.
6. A. Shah, A. Anand, Y. Sandoval, K. Lee, S. Smith, P. Adamson, A. Chapman, T. Langdon, D. Sandeman and A. Vaswani, *The Lancet*, 386 (2016) 2481.
7. B. von Jeinsen and T. Keller, *Diagnosis*, 3 (2016) 189.
8. S. Masson, P. Caironi, C. Fanizza, S. Carrer, A. Caricato, P. Fassini, T. Vago, M. Romero, G. Tognoni and L. Gattinoni, *Critical Care Medicine*, 44 (2016) 707.
9. Y. Sandoval, C.A. Herzog, S. Love, J. Cao, Y. Hu, A.H. Wu, D. Gilbertson, S. Brunelli, A. Young and R. Ler, *Clinical Chemistry*, 62 (2016) 631.
10. M. Park, M. Kim, G. Lim, S. Kang, S. An, T. Kim and J. Kang, *Lab on a Chip*, 16 (2016) 2245.
11. Y. Ding, T. Cong, X. Chu, Y. Jia, X. Hong and Y. Liu, *Anal Bioanal Chem*, 408 (2016) 5013.
12. M. Cipok, V. Deutsch, I. Elalamy, I. Kirgner, S. Kay and A. Tomer, Easily Performed Functional Flow Cytometry Assay for Heparin-Induced Thrombocytopenia and Thrombosis (HIT): Correlation with Clinical Presentation, Immunoassay and Serotonin-Release Assay, Am Soc Hematology, 2016.

13. R. Dixon, B. Davis and A. Dasgupta, *Journal of clinical Laboratory Analysis*, 30 (2016) 190.
14. R. Dixon and A. Dasgupta, *Journal of Clinical Laboratory Analysis*, 30 (2016) 1106.
15. V. Günther, D. Mueller, A. von Eckardstein and L. Saleh, *Clinical Chemistry and Laboratory Medicine (CCLM)*, 54 (2016) 823.
16. S. Barco, E. Castagnola, I. Gennai, L. Barbagallo, A. Loy, G. Tripodi and G. Cangemi, *Journal of Chemotherapy*, 28 (2016) 395.
17. J. Li, J. Lu, X. Qiao and Z. Xu, *Food Chemistry*, 221 (2017) 1285.
18. D. Yang, S. Song, K. Jun, H. Rim and W. Lee, *The Journal of the Korean Society for Transplantation*, 30 (2016) 138.
19. R. Bouquié, M. Grégoire, H. Hernando, C. Azoulay, E. Dailly, C. Monteil-Ganière, A. Pineau, G. Deslandes and P. Jolliet, *American Journal of Clinical Pathology*, 146 (2016) 119.
20. A. Lubin, S. Geerinckx, S. Bajic, D. Cabooter, P. Augustijns, F. Cuyckens and R.J. Vreeken, *Journal of Chromatography A*, 1440 (2016) 260.
21. M. Usman and G. Hempel, *SpringerPlus*, 5 (2016) 124.
22. H. Lee, Y. Ryu, L. Tutkun and E. Park, *Food and Agricultural Immunology*, 27 (2016) 367.
23. M. Zhao, G. Li, F. Qiu, Y. Sun, Y. Xu and L. Zhao, *Therapeutic Drug Monitoring*, 38 (2016) 246.
24. M. Ngavouka, P. Capaldo, E. Ambrosetti, G. Scoles, L. Casalis and P. Parisse, *Beilstein Journal of Nanotechnology*, 7 (2016) 220.
25. Z. Farka, T. Juřík, M. Pastucha, D. Kovář, K. Lacina and P. Skládal, *Electroanalysis*, 28 (2016) 1803.
26. D. Jambrec, R. Haddad, A. Lauks, M. Gebala, W. Schuhmann and M. Kokoschka, *ChemPlusChem*, 81 (2016) 604.
27. L. Li, *Int. J. Electrochem. Sci.*, 11 (2016) 4550.
28. J. Kiss, P. Pusztai, L. Óvári, K. Baán, G. Merza, A. Erdöhelyi, A. Kukovecz and Z. Kónya, *e-Journal of Surface Science and Nanotechnology*, 12 (2014) 252.
29. W. Zhang, *Spectroscopy and Spectral Analysis*, 33 (2013) 1969.
30. L. Fu, M. Sokiransky, J. Wang, G. Lai and A. Yu, *Physica. E*, 83 (2016) 146.
31. Z. Li, *Physica. E*, 77 (2013) 9438.
32. R. Fonseca, J. Ramos-Jesus, L. Kubota and R. Dutra, *Sensors*, 11 (2011) 10785.
33. S. Gomes-Filho, A. Dias, M. Silva, B. Silva and R. Dutra, *Microchemical Journal*, 109 (2013) 10.
34. R. Dutra and L. Kubota, *Clinica Chimica Acta*, 376 (2007) 114.
35. J. Chua, R. Chee, A. Agarwal, S. Wong and G.. Zhang, *Anal. Chem.*, 81 (2009) 6266.
36. S. Mayilo, M.A. Kloster, M. Wunderlich, A. Lutich, T.A. Klar, A. Nichtl, K. Kurzinger, F.D. Stefani and J. Feldmann, *Nano letters*, 9 (2009) 4558.